Journal of Theoretical Biology 361 (2014) 87–100

Contents lists available at ScienceDirect

Journal of Theoretical Biology

journal homepage: www.elsevier.com/locate/yjtbi

An ordinary differential equation model for full thickness wounds and the effects of diabetes

L.G. Bowden [a,*], P.K. Maini [a], D.E. Moulton [a], J.B. Tang [b], X.T. Wang [b], P.Y. Liu [b], H.M. Byrne [c]

[a] Wolfson Centre for Mathematical Biology, Mathematical Institute, University of Oxford, Andrew Wiles Building, Radcliffe Observatory Quarter, Woodstock Road, Oxford OX2 6GG, UK
[b] Department of Plastic Surgery, Rhode Island Hospital, Alpert Medical School of Brown University, Providence, RI, USA
[c] Department of Computer Science, University of Oxford, Wolfson Building, Parks Road, Oxford OX1 3QD, UK

HIGHLIGHTS

- A simple mathematical model of wound healing is developed.
- Asymptotic analysis of the model reveals a natural separation of timescales.
- The model is fit to data to identify differences between normal and diabetic healing.
- The model can be used to estimate the contributions of growth and contraction to dermal healing.
- Increasing dermal growth is suggested as a treatment for enhancing healing of diabetic wounds.

ARTICLE INFO

Article history:
Received 11 March 2014
Received in revised form
13 June 2014
Accepted 1 July 2014
Available online 10 July 2014

Keywords:
Epidermis
Dermis
Contraction
Tissue growth
Asymptotic analysis

ABSTRACT

Wound healing is a complex process in which a sequence of interrelated phases contributes to a reduction in wound size. For diabetic patients, many of these processes are compromised, so that wound healing slows down. In this paper we present a simple ordinary differential equation model for wound healing in which attention focusses on the dominant processes that contribute to closure of a full thickness wound. Asymptotic analysis of the resulting model reveals that normal healing occurs in stages: the initial and rapid elastic recoil of the wound is followed by a longer proliferative phase during which growth in the dermis dominates healing. At longer times, fibroblasts exert contractile forces on the dermal tissue, the resulting tension stimulating further dermal tissue growth and enhancing wound closure. By fitting the model to experimental data we find that the major difference between normal and diabetic healing is a marked reduction in the rate of dermal tissue growth for diabetic patients. The model is used to estimate the breakdown of dermal healing into two processes: tissue growth and contraction, the proportions of which provide information about the quality of the healed wound. We show further that increasing dermal tissue growth in the diabetic wound produces closure times similar to those associated with normal healing and we discuss the clinical implications of this hypothesised treatment.

1. Introduction

Wound healing is a complex process, which is far from fully understood. In diabetic wounds, intrinsic pathobiological abnormalities and extrinsic factors create an environment which is even more complex. Hallmarks of diabetes, arising from hyperglycaemia include higher risk of macrovascular diseases and neuropathy and can delay healing (American Diabetes Association, 2006) or, in extreme cases, lead to lower limb amputations (Adler et al., 1999). In the UK, wound care is estimated to cost the National Health Service approximately £1 billion a year (Hex et al., 2012). The clinical demand for treatments that can enhance wound healing, in normal and diabetic patients, is stimulating a vast amount of biomedical research.

We argue that advances in wound management will come from greater understanding of the mechanisms controlling healing. As it is often difficult to conduct in vivo investigations in a non-invasive manner, realistic mathematical models based on known cell behaviours provide a useful framework for studying wound healing. As well as mathematical models, reliable animal models that recapitulate situations of impaired wound healing are essential (Martínez-Santamaría et al., 2013). In this paper we present experimental data associated with non-diabetic and diabetic

* Corresponding author. Tel.: +44 1865 283881.
E-mail address: bowden@maths.ox.ac.uk (L.G. Bowden).

http://dx.doi.org/10.1016/j.jtbi.2014.07.001
0022-5193/

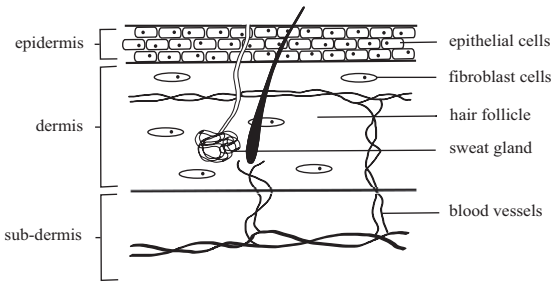

Fig. 1. Schematic of the skin. A cross-section through the three main layers of the skin. The epidermis contains layers of tightly packed epithelial cells. The dermis consists of fibroblasts, blood vessels, sweat glands and hair follicles, surrounded by elastic tissue made primarily of collagen. The sub-dermis is a fatty tissue with a network of blood vessels.

healing in mice. Motivated by the data we develop a simple mathematical model in order to determine which aspects of healing are most affected by diabetes.

Human skin is primarily divided into three layers (see Fig. 1). The outermost and thinnest layer is the epidermis. It is made from densely packed epithelial cells. Underneath is a thicker dermal layer of collagenous elastic tissue in which the main cell type is the fibroblast. Beneath the dermis lies a fatty layer called the sub-dermis, which provides the body with insulation. Partial thickness wounds affect the epidermis, may injure part of the dermis and heal mainly by epithelialisation. Of interest here are full thickness wounds in which the entire epidermis and dermis are damaged.

Normal healing of full thickness wounds in mammalian adults involves the co-ordination of a series of interrelated biochemical and biomechanical processes. It proceeds in four distinct phases, starting with haemostasis, followed by inflammation, proliferation and, finally, remodelling. In practice, these processes actually overlap. Immediately after wounding, the intrinsic tension in the surrounding tissue causes the skin to recoil (Kiehart, 1999). Haemostasis is an instantaneous response to wounding. Damaged capillaries allow blood flow into the wound causing platelets to aggregate and form a temporary seal or clot in the opening. The clot is made primarily from fibrin and is a source of the growth factors that are needed during the subsequent healing phases (Wahl et al., 1989). The growth factors in the wound space initiate the inflammatory phase, which lasts for up to a week (Jeffcoate et al., 2004), during which inflammatory cells, for example leukocytes, neutrophils and macrophages, migrate into the wound. The inflammatory cells provide chemical stimuli for the proliferative phase. Proliferation in the epidermal layer of the skin is termed epithelialisation and proceeds more quickly than dermal proliferation. A combination of proliferation and migration of epithelial cells contributes to the regeneration of an epidermal covering. In the dermis the proliferative phase is described as fibroplasia. For fibroplasia, fibroblasts diffuse into the wound space, stimulated by a family of fibroblast growth factors (FGF) produced during the inflammatory phase (Clark, 1988). The fibroblasts initiate the deposition of new extracellular matrix by producing collagen. Contraction begins approximately 2–5 days post-wounding as fibroblasts apply tensile forces to the collagen scaffold in order to shrink the wound (Monaco and Lawrence, 2003). After closure, cellular activity decreases and the collagen matrix is remodelled over a period of several months.

Diabetes is a common, life-long health condition. Worldwide there are 285 million adults diagnosed with diabetes, with this number estimated to increase by 54% by 2030 (Shaw et al., 2010). Diabetes can be categorised into type I ($\sim 10\%$) and type II ($\sim 90\%$). The former results from an inability to produce insulin, whereas the latter is an inability to efficiently use the body's insulin. This prevents the conversion of glucose into glycogen and results in high blood glucose, or hyperglycaemia. Symptoms of hyperglycaemia, such as higher risk of macrovascular disease and neuropathy, are associated with both types of diabetes (American Diabetes Association, 2006). More than 100 physiological factors contribute to wound healing deficiencies in diabetic individuals (Brem and Tomic-Canic, 2007). As mentioned above, normal wound healing requires the coordinated integration of complex biological and molecular events. In a diabetic wound these events may be disrupted, delaying healing.

Many aspects of wound healing have been the subject of mathematical and computational investigations. For example, Sherratt and Murray (1990, 1992) formulated models of epidermal healing in which reaction–diffusion equations were used to describe the spatio-temporal evolution of the epidermal cells and to compare the impact of growth factors that promote and inhibit healing. Mathematical models of full thickness wounds typically focus on dermal healing and one of the contributing processes, for example contraction (Tranquillo and Murray, 1992; Tracqui et al., 1995; Olsen et al., 1999) or tissue synthesis (Segal et al., 2012). Typically models of wound contraction are formulated as partial differential equations (PDEs) and are based on the principles of mass and momentum balance. For example, such a model may couple mass balances for the density of fibroblasts and extra-cellular matrix (ECM) with a momentum balance for the displacement of the cell-ECM continuum and constitutive laws which define the mechanical properties of the tissue. Earlier models treated the ECM as isotropic, with linear viscoelastic properties (Tranquillo and Murray, 1992). These assumptions were relaxed by Olsen et al. (1999) who viewed the ECM as an anisotropic material and studied the different roles of fibroblasts in wound contraction. More recently, Segal et al. (2012) studied the contribution of collagen accumulation in a wound to healing of the tissue. Their spatially averaged model consisted of a system of time-dependent, ordinary differential equations (ODEs). Although the complexity is reduced by adopting a spatially averaged framework, the model still has a large number of parameters that need to be determined experimentally.

The models described above have increased understanding of the specific processes involved in wound healing. However, given that these processes overlap and interact in both time and space, models that consider them in combination may provide a more realistic description of wound healing. As well as the need to consider how the different processes in healing interact, we note that it is difficult to verify detailed mathematical models with the quality of data currently available. Therefore, in this paper we develop a simple model which is cast in terms of variables that can be easily measured, namely wound areas. At a gross level, wound closure occurs due to proliferation and contraction, so these form the primary components of our model. By focussing on the net effect of these processes, rather than on the underlying mechanistic details, we develop an idealised model, containing a small number of parameters that can be used to test hypotheses about how diabetes modifies proliferation and contraction. We describe below the experiments and data which motivated this theoretical study.

In order to characterise differences in wound healing between non-diabetic and diabetic mice, we conducted a series of experiments on non-diabetic mice and mice in which type II diabetes was induced by deleting the leptin receptor gene (Coleman, 1978). Two full thickness wounds of radius 4 mm were inflicted on the backs of the mice, bilateral to the spine, using surgical scissors. Three non-diabetic and three diabetic mice were euthanised each day post-wounding; thus six wounds were harvested for each time point. This continued until wound closure, defined by closure of the epidermal gap (day 21 in the non-diabetic group and day 33 in the diabetic group). Histological samples were taken in order to measure the epidermal and dermal gaps.

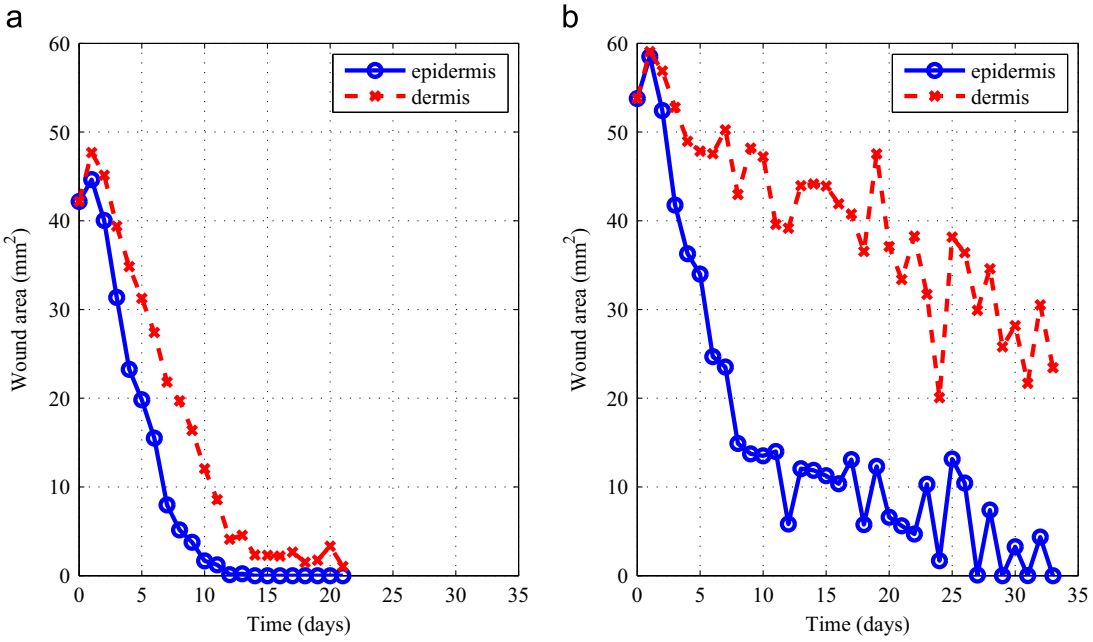

Fig. 2. Wound areas from experimental data. Average wound areas for the epidermis and the dermis in both (a) non-diabetic and (b) diabetic mice were recorded over a time period of 21 and 33 days. The sample size for each day is 6 wounds, 2 on each of the 3 mice. The initial wound radius was designed to be 4 mm and the wounds remained approximately circular throughout the experiments. The bold curve, $\mathbf{x}_e(t_i)$, gives the average epidermal area as a function of time and the dashed curve, $\mathbf{x}_d(t_i)$, the average dermal area as a function of time.

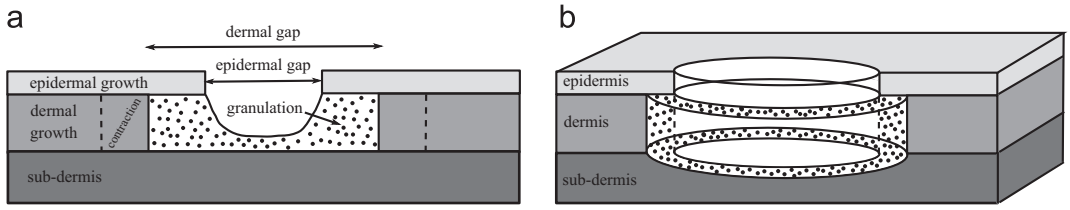

Fig. 3. Schematic representation of the wound space. The data given in Fig. 2 show the epidermal layer healing more quickly than the dermal layer, growing over the granulation tissue (given by the dotted area) and, hence, protruding into the wound space. The schematic diagram shows the arrangement of the epidermal and dermal tissues during healing, in preparation for introducing the mathematical model and its dependent variables in the next section. (a) Definition of terms and (b) radially symmetric interpretation.

From the histologies, invading fronts in both the epidermis (due to epithelial cells growing over granulation tissue) and the dermis (due to contraction and new dermal tissue) were visible. Time courses obtained by averaging the epidermal and dermal wound areas associated with the non-diabetic and diabetic groups are presented in Fig. 2. The data in Fig. 2 support the view that wound healing occurs over different timescales. For both the epidermal and dermal curves we observe a rapid increase in wound area immediately after wounding.[1] After the initial recoil the epidermal wound area gradually decreases until closure. As a consequence of granulation tissue synthesis in the dermal gap (defined by the dermal wound space), the dermal wound never fully closes. By comparing the data in Fig. 2(a) and (b) we see that the diabetic epidermis closes 19 days later than the non-diabetic epidermis, with the diabetic dermis healing even more slowly than the non-diabetic dermis. These differences indicate that a larger dermal gap remains when the diabetic wound closes, a feature which could result in a more prominent scar. We observe that, for both non-diabetic and diabetic mice, the epidermis advances more rapidly into the wound space than the dermis, forming an overhang of the epidermal layer, which grows on top of the granulation tissue synthesised in the wound space. In Fig. 3 we present a schematic diagram that clarifies how the surface areas of the wound space, the healing epidermis, and the dermis are defined and inter-related. In this diagram, the granulation tissue that is covered by new epidermis is the region of re-epithelialisation. The granulation tissue in the epidermal gap is not measured in the data presented and is therefore not discussed in this work. While it is evident from the data presented in Fig. 2 that healing in diabetic wounds is delayed, it is not clear which processes are responsible for the compromised healing.

In this paper, rather than developing a detailed model, we model in a simplified manner all the main processes that contribute to the closure of a full thickness wound: proliferation and migration of epithelial cells in the epidermis; tissue growth in the dermis; and contraction of the dermal tissue. The experimental data available to us describes how the wound areas of the epidermis and the dermis change over time. Therefore, in Section 2, we develop a model that comprises time dependent ordinary differential equations for the epidermal and dermal wound areas as the dependent variables, and that can be compared with the given data. In Section 3 we perform a focussed parameter sensitivity analysis on our model, concentrating on those parameters that are thought to be compromised in diabetic healing. By fitting the model to the experimental data from non-diabetic and diabetic wounds we are able to estimate

[1] In fact, in the non-diabetic case the wound initially contracts followed by a recoil. We do not know what causes this behaviour, so for the purpose of this work we begin the modelling after this contraction and before the recoil phase, given by the first data point in Fig. 2(a).

the system parameters and identify those which differ markedly between non-diabetic and diabetic wounds. Guided by these parameter estimates, we go on to use asymptotic techniques to show how our model can be analysed on different, well-defined timescales and how the processes that drive healing change from one timescale to the next. Finally, in Section 4 we summarise our results and explain how they could be used to suggest strategies for improving wound healing for diabetic patients.

2. The mathematical model

Since the data presented in Fig. 2 are spatially averaged, we formulate our model as a system of time dependent ordinary differential equations (ODEs), relating the changes in wound areas of the epidermis and the dermis to the dominant processes driving wound closure. The ODEs we develop represent a conservation of mass of new epidermal tissue, a conservation of mass of new dermal tissue, and a phenomenological balance of the forces acting on the dermis. When developing our model we note that the experimental wounds were formed by excising a circular region of tissue of radius 4 mm with the depth of epidermal and dermal tissues approximately 0.1 mm. For simplicity and since the radii of the wounds were much greater than their depth, we view the wounds as two-dimensional, and focus on how the areas of the epidermis and dermis change during healing by supposing that the wounds are radially symmetric, an assumption that is consistent with the histology. We will consider the time duration of healing to be from initial injury until closure of the epidermis. In this time period we do not account for remodelling of the dermis post-closure or the synthesis of granulation tissue in the wound space.

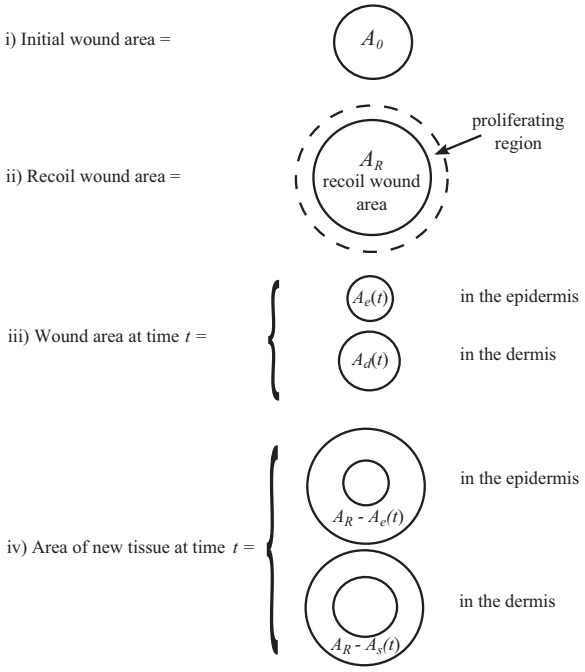

Fig. 4. Definition of wound areas and system variables. A radially symmetric interpretation of the wound areas. (i) The initial wound area of the epidermal and dermal layers is given by A_0. (ii) Following wounding the tissues in both layers retract to an area $A_R > A_0$. Proliferation in both the epidermis and the dermis is localised to a small annular region surrounding the recoiled wound. (iii) The areas of the epidermal and dermal wounds are given by the time dependent variables $A_e(t)$ and $A_d(t)$, respectively and typically $0 \le A_e(t) \le A_d(t)$. (iv) As the epidermal tissue proliferates, the area of new epidermal tissue is given by $A_R - A_e(t)$. Similarly, the area of new dermal tissue is given by $A_R - A_s(t)$, where the time dependent variable $A_s(t)$ is the area of the relaxed dermal wound. The dermal wound is also subject to contractile forces, with the amount of contraction at time t assumed to be proportional to the area difference $A_s - A_d$.

The schematic diagram presented in Fig. 4 illustrates the wound geometry that we consider and introduces the system variables. Due to the retraction (recoil) immediately following wounding, the wound increases in area from its initial wound value of A_0 to A_R, both constant values determined by the data. The areas of the epidermal and dermal wounds at time t are denoted $A_e(t)$ and $A_d(t)$, respectively. In the dermis, where we consider the combined effects of growth and contraction, it is convenient to introduce an additional variable $A_s(t) \in (A_d, A_R)$ to characterise the dermal wound. We suppose that the area of the dermal wound healed by new tissue is $A_R - A_s$ and deduce that the amount of contraction experienced by the dermal tissue will be proportional to $A_s - A_d$. We remark that both $A_e(t)$ and $A_d(t)$ are directly comparable to the epidermal and dermal data curves presented in Fig. 2, whereas $A_s(t)$ is not measurable from the data.

2.1. Mass balance for new epidermal tissue

Following Clark (1988), we suppose that the epidermal tissue heals by a combination of cell migration and proliferation. Early work on characterising proliferation in mouse epidermis revealed that mitotic activity was abnormally high in a region of width 1 mm surrounding the wound (Bullough and Laurence, 1960). However, Usui et al. (2008) showed that, in humans, migration of epithelial cells occurs at the wound margin, but that proliferation is upregulated in an area surrounding the wound, which can be up to 1 cm from the wound edge. Such behaviour was found in both non-diabetic and diabetic wounds. Upregulation of mitosis at this distance from the wound has also been observed in rat corneal epithelial wounds of varying sizes (Sandvig et al., 2009). Following Usui et al. (2008) we localise proliferation to the new epidermal tissue and a small annulus surrounding the initial wound margin. We note that, qualitatively, our results are robust to this choice (see Section 4). Cells from the wound margin are assumed to migrate towards the wound centre to assist in closing the wound. We assume further that the combined effect of these processes can be described by a modified logistic growth law in which the growth rate contains contributions from proliferation in the new wound tissue and an additional area surrounding the initial wound margin. By applying the principle of mass balance to the new epidermal tissue, $A_R - A_e(t)$, we deduce that

$$\frac{\mathrm{d}}{\mathrm{d}t}(A_R - A_e(t)) = r^*(A_R - A_e(t))\left(1 - \frac{A_R - A_e(t)}{A^*}\right), \tag{1}$$

where A^* is the carrying capacity and the growth rate r^* has the form

$$r^* = r\left(1 + \frac{\nu A_R}{A_R - A_e(t)}\right). \tag{2}$$

Here the first term, r, represents the assumed constant rate at which new epidermal tissue grows while the second term represents additional growth from the annulus surrounding the initial wound margin, the parameter ν indicating the proportion of the area, A_R, that contributes to this effect. We account for the fact that epithelial cells are known preferentially to migrate over a smooth, moist surface, such as the new dermal tissue, rather than granulation tissue (Martin, 1997; Krawczyk, 1971), by assuming that the carrying capacity A^* depends on the dermal wound area. The maximum value for the carrying capacity of new epidermal tissue is A_R, corresponding to the epidermis being fully healed ($A_e = 0$). As the dermal wound area, $A_d(t)$, decreases, the new dermal tissue offers a platform for preferential growth and migration of epidermal tissue, and the carrying capacity will increase. We therefore assume that the carrying capacity takes the following

form:

$$A^* = A_R - \gamma A_d(t), \tag{3}$$

where the parameter $\gamma \in [0,1)$ measures the degree to which the carrying capacity depends on the dermal wound area. We remark that if $\gamma = 0$, then the epidermis heals independently of the dermis, with a carrying capacity of A_R.

Substituting (2) and (3) into (1), we obtain the following ODE for $A_R - A_e(t)$, the area of new epidermal tissue at time t:

$$\frac{\mathrm{d}}{\mathrm{d}t}(A_R - A_e(t)) = r(A_R - A_e(t) + \nu A_R)\left(1 - \frac{A_R - A_e(t)}{A_R - \gamma A_d(t)}\right). \tag{4}$$

2.2. Mass balance for new dermal tissue

In the dermis we assume that contraction and growth drive healing. Both processes are regulated by fibroblasts that accumulate in the wound space following injury. When modelling proliferation in the dermis, we consider two mechanisms. Firstly, there is a basal proliferation from the healthy skin, which is localised close to the wound. Secondly, the growth rate of the new and surrounding tissue is enhanced by the amount of stretch it experiences. Such mechanosensitive behaviour is known to occur during dermal wound healing (Chiquet, 1999; Pietramaggiori, 2007). As for epidermal tissue, we assume that the growth of new dermal tissue follows a modified logistic growth law. By applying the principle of mass balance to the new dermal tissue, $A_R - A_s(t)$, we deduce that

$$\frac{\mathrm{d}}{\mathrm{d}t}(A_R - A_s(t)) = k^*(A_R - A_s(t))\left(1 - \frac{A_R - A_s(t)}{A_R}\right), \tag{5}$$

where k^* is the growth rate of the dermal tissue and A_R is the carrying capacity. As with the epidermal growth rate, we write

$$k^* = k\left(1 + \frac{\nu A_R}{A_R - A_s(t)}\right), \tag{6}$$

where the first term represents the growth rate of the new dermal tissue and the second term the contribution to growth from the annulus surrounding the initial wound margin. For simplicity we assume that the areas of the annuli surrounding the wound that contribute to epidermal and dermal tissues are identical (ν is the same in (2) and (6)). We decompose the growth rate k into basal and mechanosensitive contributions. In order to quantify the mechanosensitive contribution, we introduce the normalised area of additional tissue due to contraction, $\Psi \in [0,1)$:

$$\begin{aligned}\Psi &= \frac{\text{area of stretched tissue} - \text{area of relaxed tissue}}{\text{area of stretched tissue}} \\ &= \frac{(A_R - A_d(t) + \nu A_R) - (A_R - A_s(t) + \nu A_R)}{A_R - A_d(t) + \nu A_R} \\ &= \frac{A_s(t) - A_d(t)}{A_R - A_d(t) + \nu A_R},\end{aligned} \tag{7}$$

so that $\Psi \in [0,1)$ provides a measure of the stretch experienced by the dermal tissue ($\Psi = 0$ if $A_s = A_d$). We assume that k is a linearly increasing function of Ψ so that

$$k = k_0 + k_1\left(\frac{A_s(t) - A_d(t)}{A_R - A_d(t) + \nu A_R}\right), \tag{8}$$

where k_0 represents the assumed constant basal growth rate, and the constant of proportionality k_1 represents how mechanosensitive the dermal tissue is.

Substituting (6) and (8) into (5) we obtain the following ODE for $A_R - A_s(t)$, the area of new dermal tissue at time t:

$$\begin{aligned}\frac{\mathrm{d}}{\mathrm{d}t}(A_R - A_s(t)) = &\left(k_0 + k_1\left(\frac{A_s(t) - A_d(t)}{A_R - A_d(t) + \nu A_R}\right)\right) \\ &\times (A_R - A_s(t) + \nu A_R)\left(1 - \frac{A_R - A_s(t)}{A_R}\right).\end{aligned} \tag{9}$$

2.3. Force balance for the dermis

In order to close the model it remains to determine the evolution of $A_d(t)$. In this section we propose a phenomenological force balance to specify $A_d(t)$. Fig. 5 schematically shows the forces acting on the dermal wound. Since the timescale of interest is on the order of days, which is much longer than that associated with inertial effects, we neglect inertial terms and assume that the forces due to the elastic response, contraction and tethering are in equilibrium so that

$$0 = F_E + F_C + F_T,$$

where F_E denotes the elastic restoring force, F_C the contractile force and F_T the tethering resistance. We note that, given the assumption of radial symmetry, all forces are assumed to act in the radial direction.

When the skin is injured, the residual tension causes it to spring open to a relaxed state (Kiehart, 1999). Given that elastic fibres are distributed throughout the surrounding tissue, we assume that the elastic restoring force, which causes the recoil of the wound, is proportional to the annular area of stretched tissue surrounding the wound, $A_s(t) - A_d(t)$. We write the radial component of the elastic restoring force as

$$F_E = E(A_s(t) - A_d(t)), \tag{10}$$

where E is the elastic restoring force per unit area.

In normal, healthy tissue contraction typically begins 2–5 days post-wounding, by which time fibroblasts have migrated into the wound in response to chemical growth factors released during the inflammatory phase (Stadelmann et al., 1998). When defining the contractile force we account for this delay by introducing the continuous switch function

$$\mathcal{H}(t - t_c) = \frac{1}{2}\left[\tanh\left(\frac{t - t_c}{\theta}\right) + 1\right], \tag{11}$$

where t_c is the time delay in days and θ is the gradient of the switch. Various contraction mechanisms are thought to contribute to the reduction in wound size (Watts et al., 1958; Ehrlich, 1988; Kolodney and Wysolmerski, 1992; Nedelec et al., 2000). Here we consider the simplest and best documented: fibroblasts infiltrate the wound space and apply a contractile force, apply a contractile force causing the granulation tissue to shrink (Ehrlich, 1988; Kolodney and

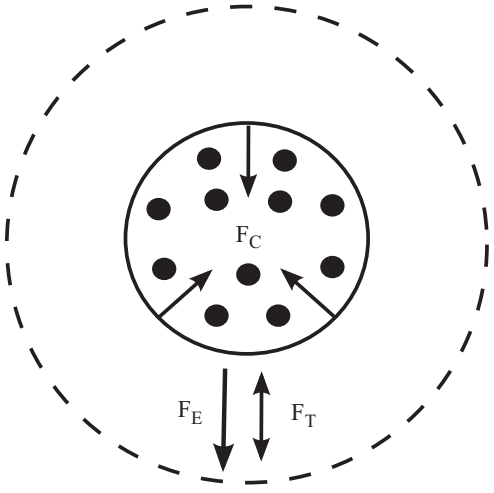

Fig. 5. Forces acting on the dermis. The inner circle represents the dermal wound area, $A_d(t)$, and the outer dashed circle the relaxed dermal wound area, $A_s(t)$. The elastic response (F_E) pulls the wound open to its relaxed state. Fibroblasts, represented by black circles, infiltrate the granulation tissue and contract (F_C) surrounding tissue in order to decrease the wound area. Friction (F_T) due to tethering to the subdermal layer acts to resist motion of the dermis.

Wysolmerski, 1992). Due to attachments between the granulation tissue and the healthy dermal tissue, this pulls the wound edge inwards, decreasing the area of the dermal wound. Since the fibroblasts migrate into the wound and can occupy the dermal wound space, we assume that the contractile force is proportional to the area of the dermal wound. We can now write the form of the radial component of the contractile force as

$$F_C = c\mathcal{H}(t-t_c)A_d, \tag{12}$$

where c is the contractile force per unit area.

Attachments between the dermal and subdermal layers resist the motion of the dermis and we assume that this tethering force is related to the velocity of the dermis. Thus, when the wound area is increasing due to the elastic response, $\mathrm{d}A_d/\mathrm{d}t > 0$ and the tethering force resists this motion. Similarly, when the wound area is decreasing due to contraction, $\mathrm{d}A_d/\mathrm{d}t < 0$ and the tethering force resists the contractile force. Guided by these observations we assume, for simplicity, that the tethering force can be written as

$$F_T = \mu\frac{\mathrm{d}A_d}{\mathrm{d}t}, \tag{13}$$

where μ is the tethering coefficient.

Combining the above assumptions, we obtain the following ODE relating the dermal wound area, $A_d(t)$, to the relaxed dermal wound area, $A_s(t)$:

$$0 = \overbrace{E(A_s-A_d)}^{\text{elastic restoring force}} - \overbrace{c\mathcal{H}(t-t_c)A_d}^{\text{delayed contractile force}} - \overbrace{\mu\frac{\mathrm{d}A_d}{\mathrm{d}t}}^{\text{tethering force}}. \tag{14}$$

2.4. Initial conditions

Following excision at $t=0$ of tissue of area A_0, the wound retracts instantaneously, exposing a larger region $A_R > A_0$. These observations, together with our assumption that the epidermis is not under tension during healing, lead us to prescribe the following initial conditions for the dependent variables:

$$A_e(0) = A_R, \quad A_s(0) = A_R, \quad A_d(0) = A_0. \tag{15}$$

The conditions in (15) close our phenomenological model of wound healing.

Eqs. (4), (9) and (14) constitute three coupled ODEs for the time evolution of the wound areas A_e, A_s and A_d. Before presenting model solutions, it is convenient to restate the governing equations, suitably rearranged to clarify their interactions:

$$\frac{\mathrm{d}A_e}{\mathrm{d}t} = -r(A_R(1+\nu)-A_e)\left(\frac{A_e-\gamma A_d}{A_R-\gamma A_d}\right),$$

$$\frac{\mathrm{d}A_s}{\mathrm{d}t} = -\left(k_0+k_1\left(\frac{A_s-A_d}{A_R(1+\nu)-A_d}\right)\right)(A_R(1+\nu)-A_s)\frac{A_s}{A_R},$$

$$\mu\frac{\mathrm{d}A_d}{\mathrm{d}t} = E(A_s-A_d)-c\mathcal{H}(t-t_c)A_d,$$

where $\mathcal{H}(t-t_c)$ is defined in (11) and the initial conditions satisfy (15).

2.5. The nondimensionalised equations

In practice, when constructing numerical and approximate analytical solutions we use a dimensionless version of Eqs. (4), (9), (14) and (15). These equations are stated below for completeness with asterisks omitted for notational simplicity (details of the nondimensionalisation are relegated to Appendix A):

$$\frac{\mathrm{d}A_e}{\mathrm{d}t} = -\lambda(1+\nu-A_e)\left(\frac{A_e-\gamma A_d}{1-\gamma A_d}\right), \tag{16a}$$

Table 1
Dimensionless parameters associated with the best fits. The dimensionless parameter values associated with the best fits to non-diabetic and diabetic data. The parameter set involved in optimisation is $\theta^{\text{ast}} = \lambda, \beta_0, \beta_1, \alpha, \gamma, \nu$.

Parameter	Physical interpretation	Non-diabetic	Diabetic
λ	Epidermal growth rate	0.5274	0.4258
β_0	Basal dermal growth rate	0.2950	0.0715
β_1	Mechanosensitive dermal growth rate	0.0124	0.0026
α	Contraction with respect to elastic response	0.2144	0.1593
γ	Epidermal dependence on dermis	0.0027	0.1868
ν	Proportion of proliferative region at wound margin	0.0904	0.1000
ϵ	Tethering with respect to elastic response	0.01	0.01
t_c	Contraction switch delay	3	3
θ	Contraction switch gradient	1	1
Kd	Ratio of initial to recoiled wound area	0.9404	0.9542

$$\frac{\mathrm{d}A_s}{\mathrm{d}t} = -\left(\beta_0+\beta_1\left(\frac{A_s-A_d}{1+\nu-A_d}\right)\right)(1+\nu-A_s)A_s, \tag{16b}$$

$$\epsilon\frac{\mathrm{d}A_d}{\mathrm{d}t} = A_s-A_d-\alpha\mathcal{H}(t-t_c)A_d, \tag{16c}$$

with initial conditions

$$A_e(0) = 1, \quad A_s(0) = 1, \quad A_d(0) = \frac{A_0}{A_R} \equiv K_d. \tag{16d}$$

The dimensionless parameters λ, β_0, β_1, ϵ, α, t_c, θ and K_d are non-negative constants whose physical interpretations are stated in Table 1.

2.6. Model behaviour

We anticipate that Eqs. (16) should reproduce the natural progression of healing with a rapid recoil phase followed by a period of cell proliferation and tissue growth, with contraction contributing at later stages. The recoil phase occurs within hours of healing. Since we are interested in the time until wound closure, our timescale of interest is on the order of days. We therefore expect that ϵ will be small in comparison to the other model parameters, representing a large elastic restoring force relative to the tethering resistant force of the dermis to the underlying layers. With $0 \ll \epsilon < 1$, we can apply the methods of matched asymptotic analysis to Eqs. (16) to verify that analysis of the model reproduces the different phases of healing on the appropriate timescales. Full details of this analysis are given in Appendix E, where our model expresses a progressive behaviour of the dominant physical mechanisms contributing to healing on each timescale, with these dominant mechanisms predicted to change in the following way:

dermal recoil → basal proliferation → contraction

→ mechanosensitive proliferation

In Fig. 6 we compare the approximate solution obtained from the asymptotic analysis with a numerical solution of the model. We observe excellent agreement between the two solutions.

In the next section we solve Eqs. (16) numerically in order to test whether the model is in good qualitative agreement with wound healing data. We further fit the model to nondimensionalised experimental data to identify the processes which differ markedly between non-diabetic and diabetic healing.

3. Numerical results

In this section we numerically solve Eqs. (16) using the stiff differential equation solver `ode15s` in MATLAB. By using a least squares fitting method we find the best fits to the data presented in Fig. 2. We further compare the parameters associated with the best fits for the non-diabetic and diabetic cases and suggest a treatment strategy that may be used to enhance healing of diabetic wounds.

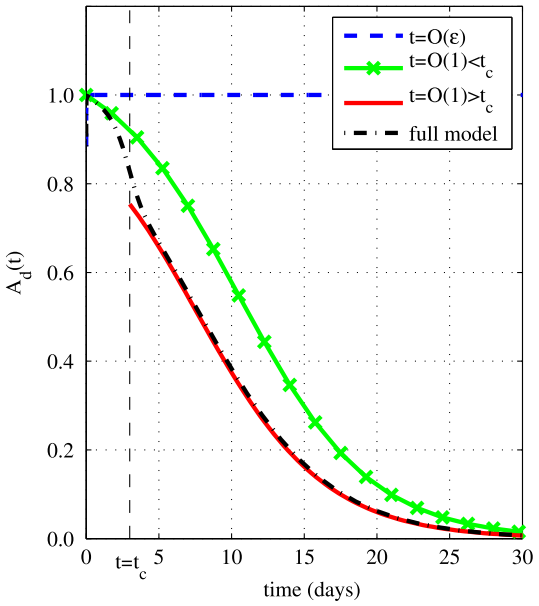

Fig. 6. Comparison of results from asymptotic analysis with numerical solutions of the full model. Leading order approximate solutions for $A_d(t)$ given by Eq. (E.2c) for $t=\mathcal{O}(\epsilon)$, Eq. (E.8b) for $t=\mathcal{O}(1)$ with $t<t_c$ and Eq. (E.8b) for $t=\mathcal{O}(1)$ with $t>t_c$ are compared with the numerical solution to the full model given by (16). The jump in solution at $t=t_c$ is a result of approximating $\mathcal{H}(t-t_c)$ with the Heaviside step function for analytical tractability (see Appendix E). Parameter values: $\theta=1, t_c=3$, $\epsilon=0.01$, $\lambda=0.2$, $\beta_0=0.2$, $\beta_1=0.2$, $\alpha=0.2$, $\gamma=0.1$, $\nu=0.1$.

3.1. Least squares analysis

Using a least squares method (see Appendix D) we fit Eqs. (16) to nondimensionalised data by exploring the parameter space given by $\Phi^*=\{\lambda,\beta_0,\beta_1,\alpha,\gamma,\nu\}$. The data in Fig. 2 are nondimensionalised by scaling the area by the maximum wound area (A_R) and time by an appropriate timescale (T), which we take to be 1 day (see Appendix B for details). The parameters $t_c=3$, $\theta=1$ and $\epsilon=0.01$ are fixed as justified by carrying out a numerical parameter sensitivity analysis (see Appendix C).

The best fits of the model to the non-diabetic and diabetic data are presented in Fig. 7 and reveal that the model fits the data well, with the non-diabetic fit being better (mean squared error, MSE=0.0017) than the diabetic fit (MSE=0.0067). This is likely due to the greater amount of noise in the diabetic data.

Table 1 displays the parameter estimates associated with the best fit curves. By comparing the non-diabetic and diabetic parameter sets, we see that epidermal growth (λ) and dermal growth (β_0 and β_1) are lower in the diabetic wounds by 20%, 75% and 80%, respectively. Contraction (α) is also compromised in diabetic healing but the decrease (25%) is less prominent than the decrease in the dermal growth parameters. Regarding the influence of the dermis on epidermal healing (γ) we observe that the diabetic estimate of γ is much greater than the non-diabetic estimate; this implies that the diabetic epidermis is more sensitive to the new dermis. Equivalently, the diabetic epidermis has a lower affinity for the granulation tissue synthesised in the wound space than the non-diabetic epidermis.

We note further that, in comparison to the other growth parameters, mechanosensitive growth (β_1) is small. By setting $\beta_1=0$ in (16) and fitting the resulting model to the data we investigate whether the data can be described without the effect of mechanosensitive growth. We calculate the MSE associated with the best fit curve in order to compare the model solutions in

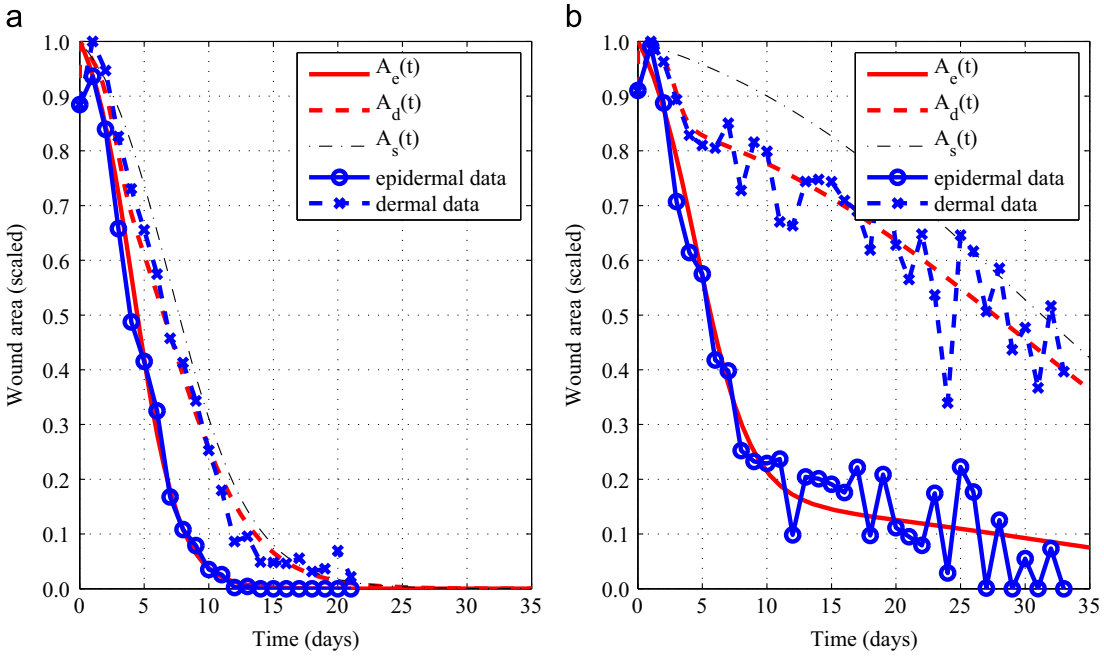

Fig. 7. Wound areas for the best fits of the model to data. The numerical solutions of (16) are fit to the data given in Fig. 2 by optimising the parameter set $\Phi^*=\{\lambda,\beta_0,\beta_1,\alpha,\gamma,\nu\}$ using a least squares analysis. The parameters $\theta=1, t_c=3$ and $\epsilon=0.01$ are fixed. (a) Best fit to the non-diabetic data with parameters $\lambda=0.5274$, $\beta_0=0.2950$, $\beta_1=0.0592$, $\alpha=0.2144$, $\gamma=0.0027$, $\nu=0.0904$. (b) Best fit to the diabetic data with parameters $\lambda=0.4258$, $\beta_0=0.0715$, $\beta_1=0.0026$, $\alpha=0.1593$, $\gamma=0.1868$, $\nu=0.1000$.

Fig. 7 to those with no mechanosensitive growth. From Table 2 we observe that the best fit curves with $\beta_1 = 0$ give the same error as those when β_1 is included in the least squares analysis.

In order to investigate whether mechanosensitive growth is small or whether our data (or model) cannot distinguish between the two types of dermal growth, we perform model simulations in which the basal growth rate of the dermis is off ($\beta_0 = 0$). The associated MSEs presented in Table 2 suggest that the model with only mechanosensitive growth ($\beta_0 = 0 < \beta_1$) describes the data less well than that with only basal growth ($\beta_1 = 0 < \beta_0$). These results suggest that the effect of mechanosensitive growth is negligible. This is because the MSE for basal growth only ($\beta_1 = 0 < \beta_0$) is the same as that with $\beta_0, \beta_1 > 0$.

When $\beta_1 = 0$, we find that β_0 is the parameter that changes most significantly between the non-diabetic and diabetic best fits. We estimate the value of β_0 with $\beta_1 = 0$ and fixed $\lambda, \alpha, \gamma, \nu$ obtained from the non-diabetic best fit (see Table 1) that gives the best fit to the diabetic data. This fit is presented in Fig. 8 with an associated MSE = 0.0170. Although the MSE associated with this fit is much greater than that when all parameters are free, the resulting solution for the dermal healing curve is qualitatively similar to that in Fig. 7(b) and the difference in error is likely due to the qualitative differences in the epidermal curves. This shows that the delay in diabetic healing can be mainly ascribed to a lower rate of basal growth.

Table 2
Comparison of error between the different types of dermal growth. The mean squared error is calculated from the best fit curves to the non-diabetic and diabetic data with either β_0 and β_1 optimised, $\beta_1 = 0$ and β_0 optimised or $\beta_0 = 0$ and β_1 optimised. The remaining parameters λ, α, γ and ν are included in the optimisation.

Type of growth	MSE	
	Non-diabetic	Diabetic
Basal and mechanosensitive ($\beta_0, \beta_1 > 0$)	0.0017	0.0067
Basal only ($\beta_1 = 0 < \beta_0$)	0.0017	0.0067
Mechanosensitive only ($\beta_0 = 0 < \beta_1$)	0.0084	0.0082

3.1.1. Processes contributing to wound closure

The main delay in healing in diabetics is closure of the dermis. From the data in Fig. 2 healing is tracked by movement of the dermal and epidermal edges. Movement of the dermal edge is due to addition of dermal tissue and contraction by fibroblasts, however, this separation of processes is not measurable by the data. The model variables for dermal healing, A_s and A_d, give an indication of the contribution to dermal healing by growth and contraction. Fig. 9 shows which area differences between the model solutions represent the contribution by area of new tissue for each process. The contribution of the individual processes measured by the best fit curves of the model for each day is given in Fig. 10.

By comparing the breakdown of processes at wound closure (defined by the data at day 14 in the non-diabetic wounds and day 33 in the diabetic wounds) we observe that the percentage healed by re-epithelialisation is much greater in the diabetic wound (approximately 30% in comparison to 10%). This large amount of granulation tissue in the dermal gap could result in severe scarring. Also, the diabetic wounds experience more contraction relative to dermal growth (10% and 60%) than the non-diabetic wounds (2% and 90%). In Section 3 we found that the contraction parameter (α) was lower in the diabetic wounds (see Table 1), therefore the diabetic tissue is less contractile than the non-diabetic tissue. However, the reduction in dermal growth in the diabetic wounds is more marked than the reduction in contraction (see Table 1), so that a greater proportion of the diabetic wounds is healed by contraction than in the non-diabetic wounds. Further, the proportion of the diabetic wounds healed by dermal growth is only 60% whereas it is almost 90% in the non-diabetic wounds.

Combining the above results, we conclude that increasing the basal growth in the dermis is likely to have the most significant effect on increasing rate of healing of diabetic wounds. In the next section we perform a parameter sensitivity analysis by varying the

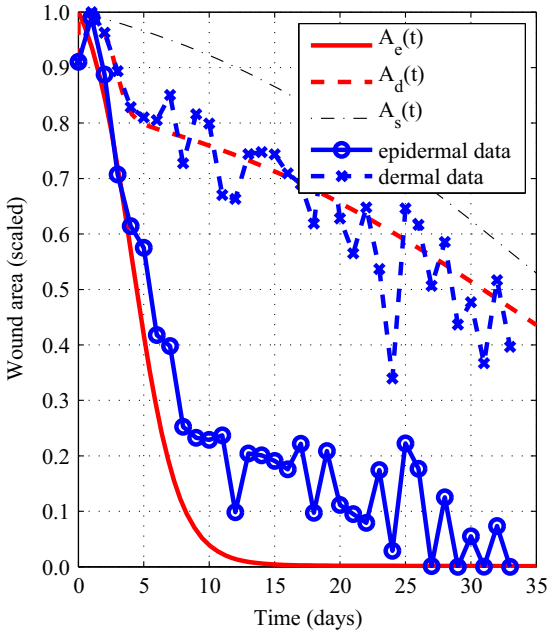

Fig. 8. Best fit to the diabetic data described by lower basal growth only. The parameter set $\Phi = \{\lambda, \alpha, \gamma, \nu\}$ is fixed according to the best fit to the non-diabetic data, given in Table 1, $\beta_1 = 0$, $\theta = 1, t_c = 3$ and $\epsilon = 0.01$ are fixed. A least squares optimisation gives $\beta_0 = 0.0645$.

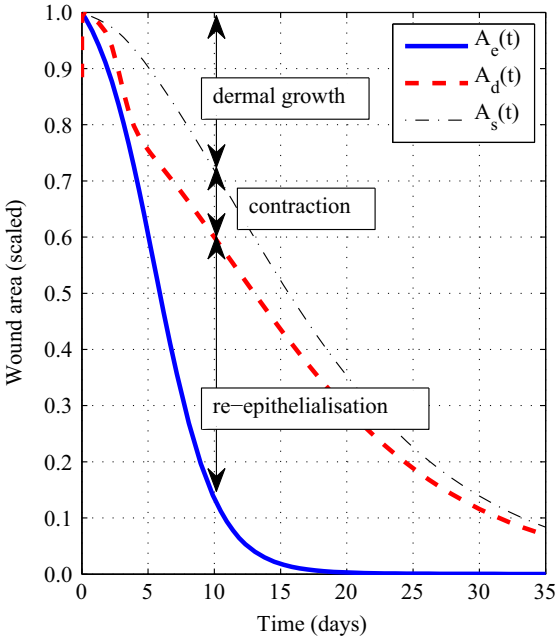

Fig. 9. Processes contributing to healing and the associated areas. The numerical solutions of (16) can be used to calculate the contribution of re-epithelialisation, contraction and dermal growth to healing. The area healed by re-epithelialisation (epidermis covering granulation tissue) is given by $A_d(t) - A_e(t)$. The area healed by contraction is given by $A_s(t) - A_d(t)$ and by dermal growth is $1 - A_s(t)$.

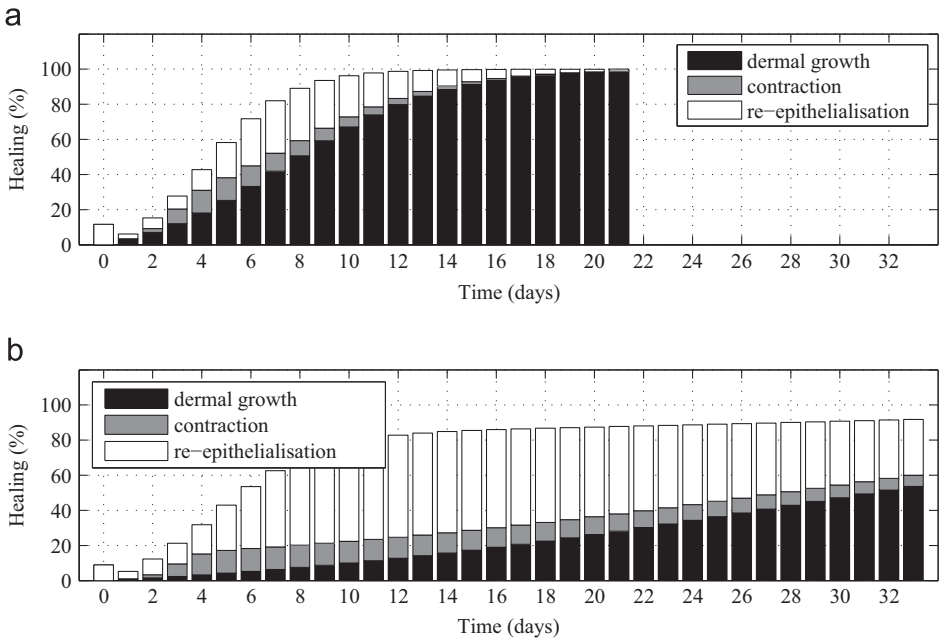

Fig. 10. Contributions from re-epithelialisation, dermal growth and dermal contraction predicted by best fits of the model to data. The numerical solutions of (16) are fit to the data given in Fig. 2 and the contributions to healing according to Fig. 9 are plotted for each day until closure. (a) Non-diabetic and (b) diabetic.

parameter β_0 to investigate the effects of increasing the basal growth on healing.

3.1.2. *Treatment intervention*

In this section we use our mathematical model to investigate a theoretical treatment for increased basal growth in the dermis, i.e. increasing the model parameter β_0. The non-diabetic wounds reach closure by day 14 (Fig. 7(a)), by which point the non-diabetic dermal curve is $A_d=0.05$. Following our analysis of reduced β_0 and parameter sensitivity we fix the parameters estimated by the diabetic best fit and increase β_0 to show how the time taken until $A_d=0.05$ changes with our theoretical treatment. β_0 is held at the increased value for all time and results are presented in Fig. 11.

From Fig. 7(a) we deduce that, in non-diabetic healing, wound closure is achieved by day 14. By increasing β_0, as shown in Fig. 11(a), from the estimated diabetic value of 0.0715 to an enhanced value of 0.34, the model predicts that the diabetic wounds will also close by day 14, normalising the dermal healing time in the diabetic wound. We observe that the curve representing increased β_0 levels off at a minimum healing time of 10 days. Similarly, the same treatment in the non-diabetic wound results in a reduced dermal healing time, with the curve having the same qualitative behaviour as that in Fig. 11(a). Fig. 11(b) shows how increasing β_0 from $\beta_0=0.0715$ to $\beta_0=0.34$ alters the contributions of contraction and growth to healing of the dermis in the diabetic wound, making them more consistent with the proportions seen in healthy, non-diabetic tissue.

Our model suggested that the contribution from mechanosensitive proliferation in the dermis was much less than that from basal proliferation. We compared the contribution to healing from contraction and dermal growth and concluded that the proportion of healing by dermal growth is much lower in the diabetic case than the non-diabetic case whereas the proportion healed by contraction was greater in the diabetic case. We investigated a treatment for increased basal growth and showed that it is theoretically possible to mimic normal healing by increasing just one of the parameters in our model (representing basal dermal growth). Combining the above results we suggest that increased dermal growth is the most effective target for treatment in order to speed up the rate of healing in diabetic wounds and normalise the proportion of healing due to contraction and dermal growth.

4. Discussion

Existing mathematical models of wound healing typically focus on epithelialisation for epidermal healing, tissue growth in dermal healing or wound contraction. In practice, wound healing involves a combination of these processes. Our work represents a simplified attempt to couple epithelialisation in the epidermis and contraction and tissue growth in the dermis. We have developed a new mathematical model which tracks changes in the epidermal and dermal areas of a wound, decreasing in time, in response to these key processes. By developing the model in tandem with experimental data, we were able to compare its dynamics directly with the data.

By fitting the model to the data we identified those parameters which differed markedly between non-diabetic and diabetic healing in mice. Our results suggest that the effects of mechanotransduction on tissue synthesis were negligible. Moreover, the dermal growth rate and the contractile force were lower in the diabetic wounds, which is consistent with the literature (Xu et al., 2013). However, the reduction in the dermal growth rate in diabetics (75% lower) is more pronounced than the reduction in contraction (25% lower), so that the contribution of contraction to healing is greater in diabetic than non-diabetic wounds (10% rather than 2%). This implies that, although both contraction and tissue growth are compromised in diabetic healing, it is likely to be more beneficial to increase growth of new tissue in the dermis than to stimulate increased contraction in order to normalise healing. These model predictions also highlight the need for additional, more detailed experiments that focus on the breakdown of dermal healing into contraction and dermal growth.

Our results suggest that the delay in diabetic healing can mainly be ascribed to a lower basal growth in the dermis. When the parameter associated with this process was increased 5-fold the model suggested that healing of the diabetic wound would more closely resemble that associated with non-diabetic wounds.

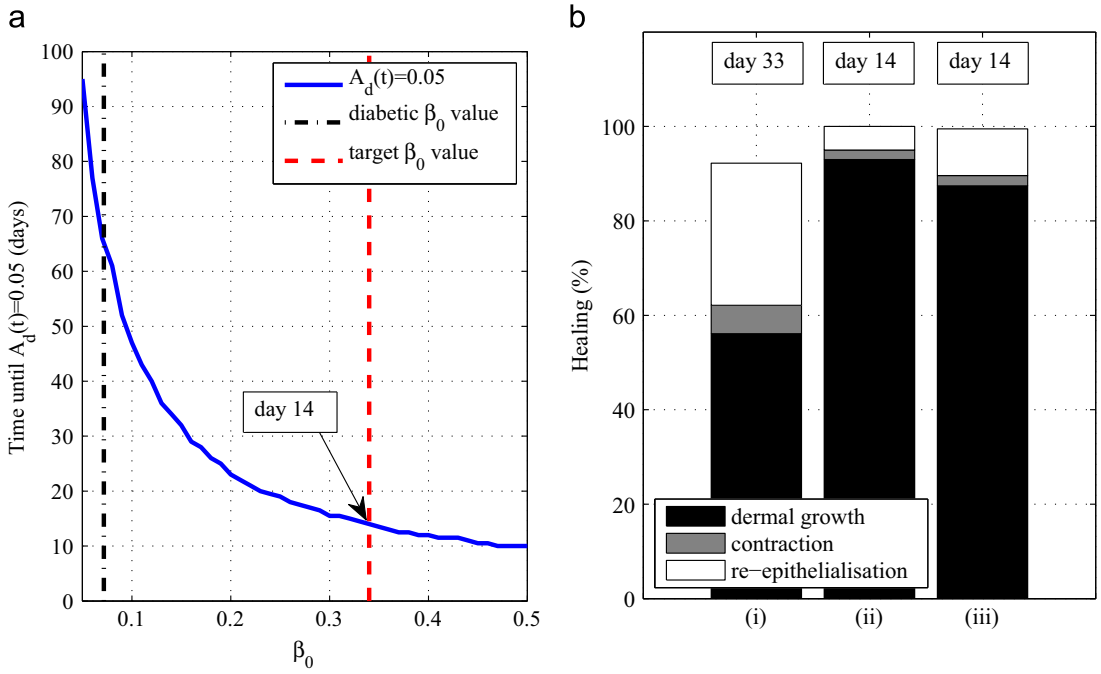

Fig. 11. Increasing β_0 as a treatment strategy. (a) Parameter sensitivity analysis showing how, for the diabetic tissue, the time for the dermal curve to reach $A_d(t)=0.05$ decreases as β_0 increases. The value of β_0 as estimated by the best fit of Eqs. (16) to the diabetic data in Fig. 2 is 0.0715 ($-\cdot-$) and the target treatment value is $\beta_0=0.34$ ($--$). By increasing β_0 to 0.34 the diabetic dermis will reach A_d=0.05 by day 14, mimicking closure of the non-diabetic wounds. All other parameters are fixed at the diabetic values in Table 1. (b) Comparison of the contributions to healing for (i) the diabetic case, (ii) the diabetic case with β_0 increased to the target value and (iii) the non-diabetic case.

There are many possible treatment applications associated with increasing the model parameter β_0. The amino acid arginine is recruited specifically for collagen synthesis. Supplemental arginine has been shown to accelerate wound healing, mainly by increasing collagen synthesis (Barbul et al., 1990). Other supplements, such as vitamin C (Ringsdorf and Cheraskin, 1982), have been shown to improve activation and stimulation of collagen synthesis. Well-established treatments, such as the application of occlusive dressings, can increase the rate of dermal epithelialisation by providing a moist wound environment (Alvarez et al., 1983). The treatments mentioned here are inexpensive and therefore readily available for treating diabetic wounds.

Through asymptotic analysis we showed that the model reproduces the normal progression of healing phases described in the biological background. The analytical descriptions of the dominant process in each healing phase could enable for a more effective analysis of healing strategies.

In our model development we assumed that the epidermal growth rate was proportional to the area of new epidermal tissue together with an annular region surrounding the initial wound. We compared these results with others for which the epidermal growth rate was proportional to the circumference of the epidermal wound (results not shown), an assumption which is consistent with Bullough and Laurence (1960). We found that the numerical solutions of the epidermal healing curve were qualitatively similar to those presented in Fig. 7. Further, by fitting this model variant to the data, our results regarding the healing of non-diabetic and diabetic wounds are unchanged.

Although the proposed model is simple, it is formulated at a level which is consistent with the data available. If we are to extrapolate our results to healing in humans we must be aware of the differences between healing in mice and humans. The most prominent of these is that healing in mice is driven mainly by contraction whereas human wounds heal mainly by re-epithelialisation. In some experiments on mice, the wounds are 'splinted' by fixing a silicon splint to the wound with adhesive (Galiano et al., 2004). As a result, contraction is slowed down and healing is more representative of human healing. By comparing our model with data taken from splinted wounds we may understand more about the compromised processes associated with diabetic healing in humans.

Parameter estimation revealed that the epidermal dependence on the dermis is greater in the diabetic wounds. Equivalently the epidermis in the diabetic wounds has a lower affinity for the granulation tissue than it does in non-diabetic wounds. This could be a property either of the epidermis or of the newly synthesised granulation tissue.

For simplicity, in this work, we have not modelled the synthesis of granulation tissue, but rather associated it with re-epithelialisation. To understand better the formation of granulation tissue and its role in epidermal migration and dermal healing, we would need to include the production of granulation in our modelling. In future work we will develop a spatially resolved model. Including spatial variation and a more detailed mechanical framework may enable to distinguish between basal and mechanosensitive growth in the dermis, while still maintaining the concepts considered in this paper and a minimal number of parameters.

Acknowledgements

L.G.B. gratefully acknowledges the UK's Engineering and Physical Sciences Research Council (EPSRC) (Award No. EP/G03706X/1) for funding through a studentship at the Systems Biology programme of the University of Oxford's Doctoral Training Centre. P.K.M. and P.Y.L. thank the Mathematical Biosciences Institute (MBI) at The Ohio State University for facilitating this research project.

Appendix A. Non-dimensionalisation

It is convenient to nondimensionalise the governing equations by introducing the following scalings for the dependent and independent variables:

$$A_e^* = \frac{A_e}{A_R}, \quad A_s^* = \frac{A_s}{A_R}, \quad A_d^* = \frac{A_d}{A_R}, \quad t^* = \frac{t}{T},$$

where T is an appropriately chosen timescale. Dimensionless parameters are defined as follows:

$$\lambda = rT, \quad \beta_0 = k_0 T, \quad \beta_1 = k_1 T, \quad \alpha = \frac{c}{E}, \quad \epsilon = \frac{\mu}{ET}, \quad t_c^* = \frac{t_c}{T}, \quad \theta^* = \frac{\theta}{T}.$$

By dropping the asterisks for convenience we can write the non-dimensionalised equations as follows:

$$\frac{dA_e}{dt} = -\lambda(1+\nu-A_e)\left(\frac{A_e-\gamma A_d}{1-\gamma A_d}\right), \tag{A.1a}$$

$$\frac{dA_s}{dt} = -\left(\beta_0+\beta_1\left(\frac{A_s-A_d}{1+\nu-A_d}\right)\right)(1+\nu-A_s)A_s, \tag{A.1b}$$

$$\epsilon\frac{dA_d}{dt} = A_s - A_d - \alpha\mathcal{H}(t-t_c)A_d, \tag{A.1c}$$

with initial conditions

$$A_e(0) = 1, \quad A_s(0) = 1, \quad A_d(0) = \frac{A_0}{A_R} \equiv K_d. \tag{A.1d}$$

Appendix B. Parameter estimation

In this section we discuss the estimation of A_R, T and the dimensionless parameters which are fixed for the least squares analysis. The value A_R is the maximum area of the wound, which, from the data, is 47.6816 mm^2 in the non-diabetic and 59.0705 mm^2 in the diabetic wounds. T is taken to be 1 day, which is approximately the cell doubling time for both epithelial cells and fibroblasts (Shi and King, 2005; Ghosh et al., 2007).

The value ϵ represents a measure of friction relative to the elastic response. We assume that the elastic response is much greater than the tethering so that the wound springs open to its relaxed size and hence $\epsilon \ll 1$. The magnitude of ϵ determines the non-dimensionalised time-frame over which the wound recoils. This occurs very quickly, although the recoil data presented in Fig. 2 are given for days 0 and 1 only, hence the magnitude of ϵ is unknown. We therefore take $\epsilon = 0.01$ (see Table B1 for the corresponding time-frame for recoil) and note that the choice of ϵ does not affect our analysis but influence the speed of recoil only. For a more representative value, additional data between days 0 and 1 would be required. The delay for contraction is known to be approximately 2–5 days post-wounding (Monaco and Lawrence, 2003). The parameter t_c represents the time (in days) at which $\mathcal{H}(t-t_c) = 0.5$. We therefore assume that $t_c = 3$ and fix θ as follows. We consider the gradient of the contraction switch and assign $\theta = 1$ such that the continuous switch represents a period of 4 days from which contraction begins to activate until it has reached close to its maximum. This 4-day period (day 1–5) represents the time for which the fibroblasts infiltrate the granulation tissue in the wound space.

Table B1
Time taken for maximum recoil and corresponding magnitudes of ϵ. Using the model given by (16) we calculate the time taken for $A_d(t)$ to reach maximum recoil for the given magnitudes of ϵ.

Timescale	ϵ
Days	$\mathcal{O}(1)$
Hours	$\mathcal{O}(10^{-2})$
Minutes	$\mathcal{O}(10^{-4})$
Seconds	$\mathcal{O}(10^{-6})$

Appendix C. Numerical parameter sensitivity analysis

Given the model defined by (16) with parameter set $\Phi = \{\phi_1, \phi_2, \ldots, \phi_n\}$ we define the sensitivity $S(t)$, of the solution $A(t,\Phi)$, with respect to the parameter ϕ_k by the following formula:

$$S(t) = \frac{\text{normalised change in } A(t;\Phi)}{\text{normalised change in } \phi_k} = \frac{\Delta A(t;\Phi)}{\Delta\phi_k}\frac{\phi_k}{A(t,\Phi)}. \tag{C.1}$$

Since we have obtained numerical solutions, (C.1) is a discretised analogue of the method often used in parameter sensitivity analysis (Dickinson and Gelinas, 1976), where partial derivatives of the solutions with respect to the parameters are calculated. The parameter ϕ_k is varied by $\pm 60\%$ and the normalised change in $A(t,\Phi)$ is defined as the absolute value of the difference in the solution at time t. In Fig. C1 we present the average (over time) sensitivity of A_e and A_d to each of the parameters, defined by

$$\overline{S} = \frac{1}{T}\sum_{i=0}^{i=T} S(t_i). \tag{C.2}$$

The model parameters we are interested in comparing are those which represent proliferation in the epidermis (λ) and growth (β_0, β_1) and contraction (α) in the dermis. We therefore fix $\theta = 1$, $t_c = 3$ and $\epsilon = 0.01$, since they have a low sensitivity in comparison to the other parameters (see Appendix B). Given the relatively high sensitivity of γ and ν we optimise these together with the parameters of interest. The parameter set optimised in the least squares analysis is therefore $\Phi^* = \{\lambda, \beta_0, \beta_1, \alpha, \gamma, \nu\}$.

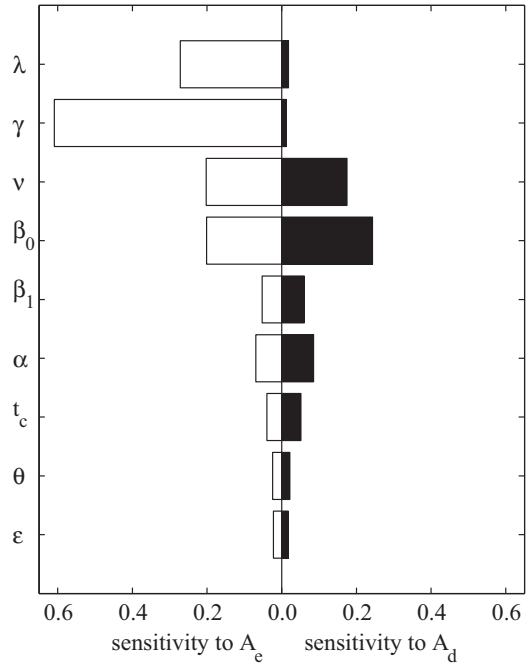

Fig. C1. Average parameter sensitivity to the model solutions. Numerical parameter sensitivity to the solutions $A_e(t)$ and $A_d(t)$ of (16) are averaged using Eqs. (C.1) and (C.2) for the parameter set $\Phi = \{\lambda, \beta_0, \beta_1, \alpha, \gamma, \theta, t_c, \epsilon, \nu\}$.

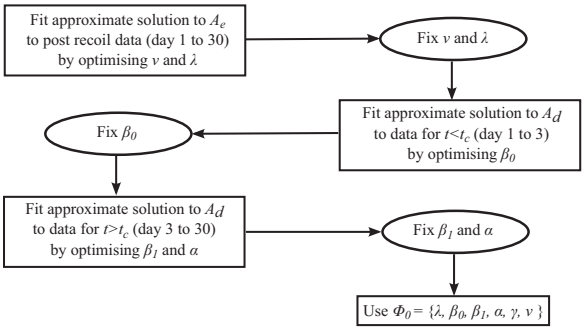

Fig. D1. Flowchart of the method for selecting an initial parameter set. Using the least squares analysis we fit the approximate solutions presented in Appendix E, to the associated subset of data, to find an initial parameter set Φ_0 for the least squares analysis of the full model. Since $\gamma \in (0,1)$ we take $\gamma_0 = 0.1$.

Appendix D. Least squares method

Given the model solutions $A_e(t;\Phi)$ and $A_d(t;\Phi)$, where Φ is the set of model parameters, and the data sets $\mathbf{x}_e(t_i)$ and $\mathbf{x}_d(t_i)$, we aim to find $\Phi^* \subseteq \Phi$ such that it minimises the sum of errors squared (MSE):

$$\mathrm{MSE} = \min_{\Phi^*}\left[\frac{1}{k}\sum_{i=1}^{k}(|x_e(t_i)-A_e(t_i,\Phi)|+|x_d(t_i)-A_d(t_i,\Phi)|)^2\right]. \tag{D.1}$$

This least squares method is implemented using the `lsqnonlin` function in MATLAB and requires a starting vector of parameter values Φ_0. In order to determine Φ_0 we fit the approximate solutions for each timescale found in Appendix E to the relevant subset of the data. By doing this we reduce the number of parameters in the least squares analysis and hence the method is less likely to settle at a local minimum. The method for choosing Φ_0 is summarised in the flowchart in Fig. D1.

Appendix E. Asymptotic analysis

The natural timescales of interest are the recoiling of the wound, which occurs for $t=\mathcal{O}(\epsilon)$; before contraction is switched on when $t<t_c$; and, when contraction is activated for $t\geq t_c$. In order for Eqs. (16) to be analytically tractable we approximate the continuous switch function, $\mathcal{H}(t-t_c)$, by the Heaviside step function, $H(t-t_c)$, that is, $H=0$ for $t<t_c$ and $H=1$ for $t\geq t_c$. This means that contraction is either on or off. We note that, in the limit as $\theta\to 0$, then $\mathcal{H}(t-t_c)\to H(t-t_c)$ and the numerical solution of (16) tends to the asymptotic solution (results not shown). From the estimation of parameters ϵ is very small and we exploit this to find asymptotic expansions of the model solutions, $A_e(t), A_s(t)$ and $A_d(t)$.

E.1. Approximate solutions

We consider the model given by (16) and replace the continuous contraction switch, $\mathcal{H}(t-t_c)$, with the Heaviside function, $H(t-t_c)$, in order to clearly separate the two timescales $t<t_c$ and $t\geq t_c$ and for analytical tractability. The system we look to analyse is therefore

$$\frac{dA_e}{dt} = -\lambda(1+\nu-A_e)\left(\frac{A_e-\gamma A_d}{1-\gamma A_d}\right), \tag{E.1a}$$

$$\frac{dA_s}{dt} = -\left(\beta_0+\beta_1\left(\frac{A_s-A_d}{1+\nu-A_d}\right)\right)(1+\nu-A_s)A_s, \tag{E.1b}$$

$$\epsilon\frac{dA_d}{dt} = A_s - A_d - \alpha H(t-t_c)A_d, \tag{E.1c}$$

where the initial conditions satisfy (16d).

Since ϵ is small this system gives rise to a boundary layer for $t=\mathcal{O}(\epsilon)$ in which dA_d/dt is large and hence the solution $A_d(t)$ is rapidly evolving. We first seek the solution on this fast timescale, which we call the inner solution (inside the boundary layer).

E.1.1. Inner solution: $t=\mathcal{O}(\epsilon)$

By considering $t=\mathcal{O}(\epsilon)$ we rescale time such that $t=\epsilon\tau$. Noting that, for small times ($t=\epsilon\tau \ll t_c$) $H=0$ and substituting in the fast time variable, τ, (E.1) becomes

$$\frac{d\overline{A}_e}{d\tau} = -\epsilon\lambda(1+\nu-\overline{A}_e)\left(\frac{\overline{A}_e-\gamma\overline{A}_d}{1-\gamma\overline{A}_d}\right), \tag{E.2a}$$

$$\frac{d\overline{A}_s}{d\tau} = -\epsilon\left(\beta_0+\beta_1\left(\frac{\overline{A}_s-\overline{A}_d}{1+\nu-\overline{A}_d}\right)\right)(1+\nu-\overline{A}_s)\overline{A}_s, \tag{E.2b}$$

$$\frac{d\overline{A}_d}{d\tau} = \overline{A}_s - \overline{A}_d, \tag{E.2c}$$

where the initial conditions satisfy (16d). Substituting power series expansions for the variables into (E.2) and equating powers of ϵ we obtain the following asymptotic expansions:

$$\overline{A}_e(\tau) = 1-\epsilon\nu\lambda\tau+\mathcal{O}(\epsilon^2), \tag{E.3a}$$

$$\overline{A}_s(\tau) = 1-\epsilon[\nu\beta_0\tau-\nu\beta_1\log((1-K_d)e^{-\tau}+\nu)]+\mathcal{O}(\epsilon^2), \tag{E.3b}$$

$$\begin{aligned}\overline{A}_d(\tau) = {} & 1-(1-K_d)e^{-\tau}-\epsilon[\nu\beta_0(\tau+e^{-\tau}-1)\\ & -\beta_1((1-K_d)e^{-\tau}+\nu)\log((1-K_d)e^{-\tau}+\nu)\\ & -\beta_1(1-K_d)e^{-\tau}\tau+\beta_1e^{-\tau}(1-K_d+\nu)\log(1-K_d+\nu)]+\mathcal{O}(\epsilon^2).\end{aligned} \tag{E.3c}$$

On this timescale, we deduce that at leading order, $\overline{A}_d$ increases exponentially, representing the recoil of the wound. We also deduce that $\overline{A}_s$ and $\overline{A}_e$ remain constant. The expansions begin to break down at $\mathcal{O}(\epsilon)$, implying that for $t=\mathcal{O}(1)$ the solutions will involve another process. The dominant process here is retraction of the dermis.

E.1.2. Outer solution: $t<t_c$

As $\tau\to\infty$ we approach the edge of the boundary layer and return to the original time variable t. On this timescale we solve for the outer solution by considering (E.1) and noting that $H=0$ since $t<t_c$. For the initial conditions we consider the limit as $\tau\to\infty$ of the solutions in the boundary layer (before the expansion breaks down, i.e. to $\mathcal{O}(1)$):

$$\hat{A}_e(0) = \lim_{\tau\to\infty}\overline{A}_e(\tau) = 1,$$

$$\hat{A}_s(0) = \lim_{\tau\to\infty}\overline{A}_s(\tau) = 1,$$

$$\hat{A}_d(0) = \lim_{\tau\to\infty}\overline{A}_d(\tau) = 1.$$

In order to obtain an analytic solution we solve for $\gamma=0$. Substituting power series expansions in ϵ into (E.1) and equating powers of ϵ we obtain

$$\hat{A}_e(t) \approx \frac{1+\nu}{1+\nu e^{\lambda(1+\nu)t}}, \tag{E.4a}$$

$$\hat{A}_s(t) = \frac{1+\nu}{1+\nu e^{\beta_0(1+\nu)t}}+\epsilon\hat{A}_{s_1}+\mathcal{O}(\epsilon^2), \tag{E.4b}$$

$$\hat{A}_d(t) = \frac{1+\nu}{1+\nu e^{\beta_0(1+\nu)t}}+\epsilon\hat{A}_{d_1}+\mathcal{O}(\epsilon^2), \tag{E.4c}$$

where

$$\hat{A}_{s_1}(t) = \frac{\beta_1 \nu (1+\nu)^2 e^{\beta_0(1+\nu)t}}{(1+\nu e^{\beta_0(1+\nu)t})^2} \log\left(\frac{(1+\nu)e^{\beta_0(1+\nu)t}}{1+\nu e^{\beta_0(1+\nu)t}}\right), \tag{E.5a}$$

$$\hat{A}_{d_1}(t) = \frac{\nu(1+\nu)^2 e^{\beta_0(1+\nu)t}}{(1+\nu e^{\beta_0(1+\nu)t})^2}\left(\beta_0 + \beta_1 \log\left(\frac{(1+\nu)e^{\beta_0(1+\nu)t}}{1+\nu e^{\beta_0(1+\nu)t}}\right)\right). \tag{E.5b}$$

On this timescale, we deduce that at leading order, $\hat{A}_e$ and $\hat{A}_s$ decrease logistically, representing a proliferative phase in both the epidermis and the dermis. The rates are proportional to $1+\nu$, which represents the area of the active region surrounding the wound. Here we see only basal growth in the dermis since contraction is not yet active, and to leading order the solution $\hat{A}_d$ is equivalent to $\hat{A}_s$. However, to $\mathcal{O}(\epsilon)$, $\hat{A}_d$ and $\hat{A}_s$ differ, indicating that another process is affecting the solutions. By the appearance of the parameter β_1 in $\hat{A}_{s_1}$ and $\hat{A}_{d_1}$, we anticipate that on the next timescale mechanosensitive growth will contribute. The dominant process here is basal growth.

E.1.3. Transition layer: $t \approx t_c$

As $t \to t_c$ contraction becomes active. We note that for $t \approx t_c$, the change in H will affect the solution $A_d(t)$. We write power series expansions for $A_s(t) = \check{A}_s(\epsilon, t)$ and $A_d(t) = \check{A}_d(\epsilon, t)$. Substituting into (E.1b) with $H=1$ and equating powers of ϵ we obtain

$$\check{A}_e(t) = \hat{A}_e(t), \tag{E.6a}$$

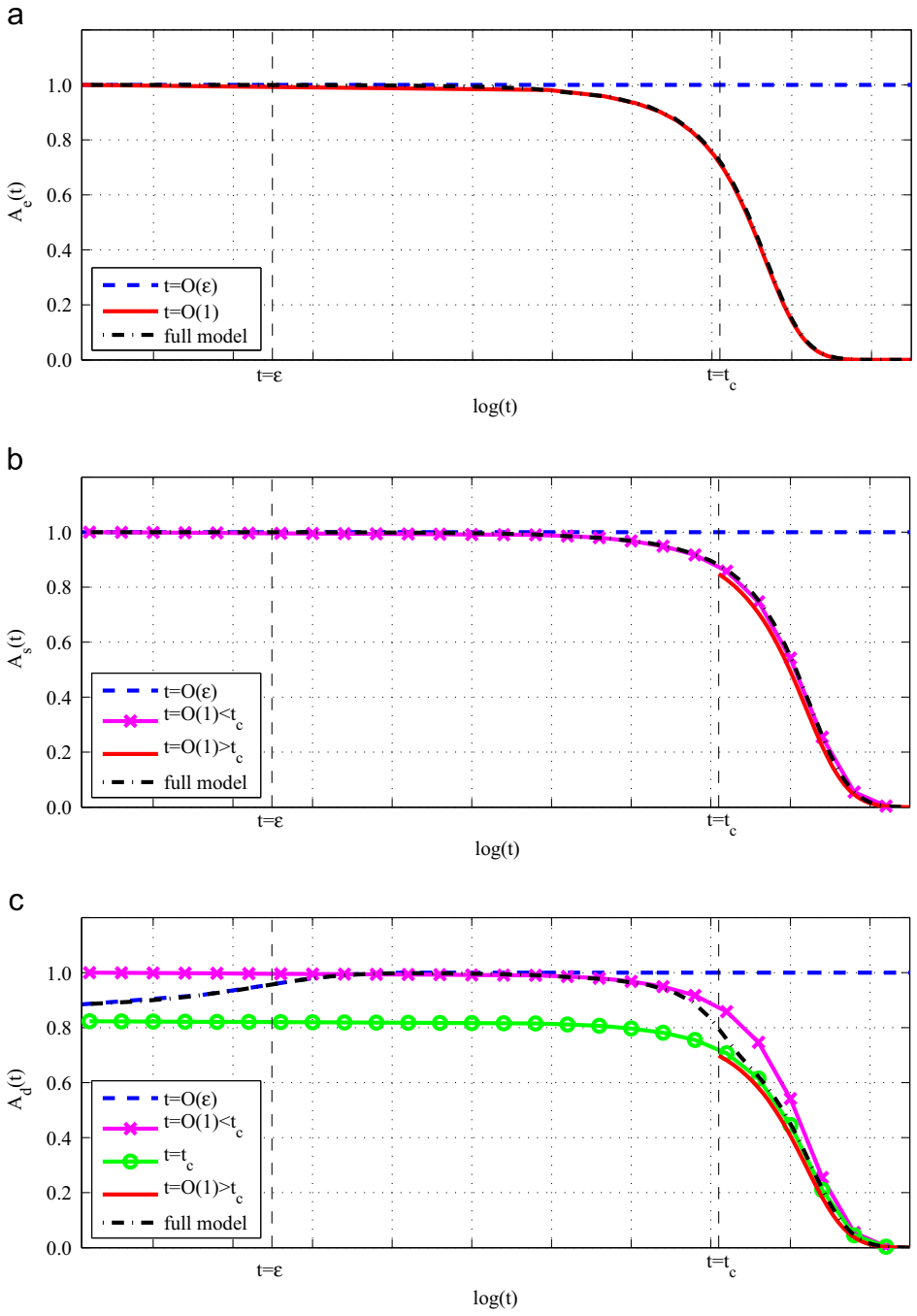

Fig. E1. Comparison of approximate solutions with numerical solution of the full model. Leading-order, approximate solutions for (a) $A_e(t)$, (b) $A_s(t)$ and (c) $A_d(t)$ on each timescale are shown to be in good agreement with numerical solutions to the full model given by (16). Parameter values: $\theta = 1, t_c = 3$, $\epsilon = 0.01$, $\lambda = 0.55274$, $\beta_0 = 0.2950$, $\beta_1 = 0.0124$, $\alpha = 0.2144$, $\gamma = 0.0027$, $\nu = 0.0904$.

$$\check{A}_s(t) = \hat{A}_s(t), \tag{E.6b}$$

$$\check{A}_d(t) = \frac{\hat{A}_{s_0}}{1+\alpha} + \epsilon\left(\frac{\hat{A}_{s_1} - \frac{1}{1+\alpha}\frac{d\hat{A}_{s_0}}{dt}}{1+\alpha}\right) + \mathcal{O}(\epsilon^2). \tag{E.6c}$$

where,

$$\hat{A}_{s_0}(t) = \frac{1+\nu}{1+\nu e^{\beta_0(1+\nu)t}},$$

and $\hat{A}_{s_1}(t)$ is given by (E.5a). As contraction becomes active, the solutions $\check{A}_e$ and $\check{A}_s$ remain the same as those for $t < t_c$, whereas $\check{A}_d$ experiences a jump in the solution across $t = t_c$. We now observe a contribution to reduction in dermal wound size due to contraction. Now that contraction is on we expect that the difference $\check{A}_s - \check{A}_d$ will stimulate mechanosensitive proliferation.

E.1.4. Outer solution: $t > t_c$

Contraction is now activated as $t > t_c$. We note that this will affect the solutions A_s and A_d but since we have taken $\gamma = 0$ in order to obtain analytical solutions, A_e will remain the same. We write power series expansions in ϵ for $A_s(t) = \tilde{A}_s(\epsilon, t)$ and $A_d(t) = \tilde{A}_d(\epsilon, t)$ and take initial conditions which satisfy the previous solutions for $t = t_c$:

$$\tilde{A}_s(0) = \check{A}_s(t_c),$$
$$\tilde{A}_d(0) = \check{A}_d(t_c).$$

Substituting $\tilde{A}_s(\epsilon, t)$ and $\tilde{A}_d(\epsilon, t)$ into (E.1b) and (E.1c) and equating powers of ϵ we obtain

$$\frac{d\tilde{A}_{s_0}}{dt} = -\left(\beta_0 + \alpha\beta_1\left(\frac{\tilde{A}_{d_0}}{1+\nu-\tilde{A}_{d_0}}\right)\right)(1+\nu-\tilde{A}_{s_0})\tilde{A}_{s_0}, \tag{E.8a}$$

$$\tilde{A}_{d_0} = \frac{\tilde{A}_{s_0}}{1+\alpha}. \tag{E.8b}$$

We observe that the equation for $\tilde{A}_{s_0}$ now depends on β_1, indicating that, to $\mathcal{O}(1)$, mechanosensitive proliferation is contributing to the reduction in dermal wound area.

E.2. Analytical results

We present the approximate solutions on the various timescales in Fig. E1 and on the same figures we present the numerical solution to the full model given by (16) for comparison (see Section 3). We use the parameters found for the best fit to the non-diabetic data given in Fig. 7(a). Within the correct timescale, the asymptotic solutions to first order are a good approximation to the numerical solution of the full model. Outside the timescale on which the solutions are valid the error between the asymptotic solution and the numerical solution to the full model increases. We can therefore deduce that the approximate solutions at leading order describe the dominant processes occurring on each relevant timescale.

References

Adler, A.I., Boyko, E.J., Ahroni, J.H., Smith, D.G., 1999. Lower-extremity amputation in diabetes. The independent effects of peripheral vascular disease, sensory neuropathy, and foot ulcers. Diabetes Care 22 (7), 1029–1035.

Alvarez, O.M., Mertz, P.M., Eaglstein, W.H., 1983. The effect of occlusive dressings on collagen synthesis and re-epithelialization in superficial wounds. J. Surg. Res. 35 (2), 142–148.

American Diabetes Association, 2006. Diagnosis and classification of diabetes mellitus. Care 29 (S), S43–S48.

Barbul, A., Lazarou, S.A., Efron, D.T., Wasserkrug, H.L., Efron, G., 1990. Arginine enhances wound healing and lymphocyte immune responses in humans. Surgery 108 (2), 331–337.

Brem, H., Tomic-Canic, M., 2007. Cellular and molecular basis of wound healing in diabetes. J. Clin. Invest. 117 (5), 1219–1222.

Bullough, W.S., Laurence, E.B., 1960. The control of epidermal mitotic activity in the mouse. Proc. R. Soc. B. 151 (945), 517–536.

Chiquet, M., 1999. Regulation of extracellular matrix gene expression by mechanical stress. Matrix Biol. 18 (5), 417–426.

Clark, R.A.F., 1988. The Molecular and Cellular Biology of Wound Repair. Plenum, New York.

Coleman, D.L., 1978. Obese and diabetes: two mutant genes causing diabetes-obesity syndromes in mice. Diabetologia 14 (3), 141–148.

Dickinson, R.P., Gelinas, R.J., 1976. Sensitivity analysis of ordinary differential equation systems: a direct method. J. Comput. Phys. 21 (2), 123–143.

Ehrlich, H.P., 1988. Wound closure: evidence of cooperation between fibroblasts and collagen matrix. Eye 2 (2), 149–157.

Galiano, R.D., Michaels, J., Dobryansky, M., Levine, J.P., Gurtner, G.C., 2004. Quantitative and reproducible murine model of excisional wound healing. Wound Repair Regen. 12 (4), 485–492.

Ghosh, K., Pan, Z., Guan, E., Ge, S., Liu, Y., Nakamura, T., Ren, X., Rafailovich, M., Clark, R.A.F., 2007. Cell adaptation to a physiologically relevant ECM mimic with different viscoelastic properties. Biomaterials 28 (4), 671–679.

Hex, N., Bartlett, C., Wright, D., Taylor, M., Varley, D., 2012. Estimating the current and future costs of type 1 and type 2 diabetes in the UK, including direct health costs and indirect societal and productivity costs. Diabetic Med. 29 (7), 855–862.

Jeffcoate, W.J., Price, P., Harding, K.G., 2004. Wound healing and treatments for people with diabetic foot ulcers. Diabetes Metab. Res. 20 (Suppl. 1), S78–S89.

Kiehart, D.P., 1999. Wound healing: the power of the purse string. Curr. Biol. 9 (16), R602–R605.

Kolodney, M.S., Wysolmerski, R.B., 1992. Isometric contraction by fibroblasts and endothelial cells in issue culture: a quantitative study. J. Cell Biol. 117 (1), 73–82.

Krawczyk, W.S., 1971. A pattern of epidermal cell migration during wound healing. J. Cell Biol. 49 (2), 247–263.

Martin, P., 1997. Wound healing: aiming for perfect skin regeneration. Science 276 (5309), 75–81.

Martínez-Santamaría, L., Conti, C.J., Llames, S., García, E., Retamosa, L., Holguín, A., Illera, N., Duarte, B., Camblor, L., Llaneza, J.M., Jorcano, J.L., Larcher, F., Meana, Á., Escámez, M.J., Del Río, M., 2013. The regenerative potential of fibroblasts in a new diabetes-induced delayed humanised wound healing model. Exp. Dermatol. 22 (3), 195–201.

Monaco, J.L., Lawrence, W.T., 2003. Acute wound healing an overview. Clin. Plast. Surg. 30 (1), 1–12.

Nedelec, B., Ghahary, A., Scott, P.G., Tredget, E.E., 2000. Control of wound contraction. Basic and clinical features. Hand Clin. 16 (2), 289–302.

Olsen, L., Maini, P.K., Sherratt, J.A., Dallon, J., 1999. Mathematical modelling of anisotropy in fibrous connective tissue. Math. Biosci. 158 (2), 145–170.

Pietramaggiori, G., 2007. Tensile forces stimulate vascular remodeling and epidermal cell proliferation in living skin. Ann. Surg. 246 (5), 896–902.

Ringsdorf, W.M., Cheraskin, E., 1982. Vitamin C and human wound healing. Oral Surg. Oral Med. Oral Pathol. 53 (3), 231–236.

Sandvig, K.U., Haaskjold, E., Bjerknes, R., Refsum, S.B., Kravik, K., 2009. Cell kinetics of conjunctival and corneal epithelium during regeneration of different-sized corneal epithelial defects. Acta Ophthalmol. 72 (1), 43–48.

Segal, R.A., Diegelmann, R.F., Ward, K.R., Reynolds, A., 2012. A differential equation model of collagen accumulation in a healing wound. Bull. Math. Biol. 74 (9), 2165–2182.

Shaw, J.E., Sicree, R.A., Zimmet, P.Z., 2010. Global estimates of the prevalence of diabetes for 2010 and 2030. Diabetes Res. Clin. Pract. 87 (1), 4–14.

Sherratt, J.A., Murray, J.A., 1990. Models of epidermal wound healing. Proc. Biol. Sci. 241 (1300), 29–36.

Sherratt, J.A., Murray, J.D., 1992. Epidermal wound healing: the clinical implications of a simple mathematical model. Cell Transplant. 1 (5), 365–371.

Shi, Q., King, R.W., 2005. Chromosome nondisjunction yields tetraploid rather than aneuploid cells in human cell lines. Nature 437 (7061), 1038–1042.

Stadelmann, W.K., Digenis, A.G., Tobin, G.R., 1998. Physiology and healing dynamics of chronic cutaneous wounds. Am. J. Surg. 176 (2), 26S–38S.

Tracqui, P., Woodward, D.E., Cruywagen, G.C., Cook, J., Murray, J.D., 1995. A mechanical model for fibroblast-driven wound healing. J. Biol. Syst. 3 (4), 1075–1084.

Tranquillo, R.T., Murray, J.D., 1992. Continuum model of fibroblast-driven wound contraction: inflammation-mediation. J. Theor. Biol. 158 (2), 135–172.

Usui, M.L., Mansbridge, J.N., Carter, W.G., Fujita, M., Olerud, J.E., 2008. Keratinocyte migration, proliferation, and differentiation in chronic ulcers from patients with diabetes and normal wounds. J. Histochem. Cytochem. 56 (7), 687–696.

Wahl, S.M., Wong, H., McCartney-Francis, N., 1989. Role of growth factors in inflammation and repair. J. Cell. Biochem. 40 (2), 193–199.

Watts, G.T., Grillo, H.C., Gross, J., 1958. Studies in wound healing: II. The role of granulation tissue in contraction. Ann. Surg. 148 (2), 153–160.

Xu, F., Zhang, C., Graves, D.T., 2013. Abnormal cell responses and role of TNF-α in impaired diabetic wound healing. Biomed. Res. Int. 1, 1–9.